In-Flight Magnetometer Calibration with Temperature Compensation for PHOENIX CubeSat

Ming-Yang Hong
Department of Electrical Engineering, National Cheng Kung University
No.1, Daxue Rd., 70101 TAINAN, TAIWAN
hmi60117@gmail.com

Faculty Advisor: Jyh-Ching Juang
Department of Electrical Engineering, National Cheng Kung University

ABSTRACT

PHOENIX is one of 2U CubeSats in QB50 project. The CubeSat was designed, assembled, integrated, tested and operated by National Cheng Kung University, Taiwan. After the deployment from International Space Station (ISS) in May 2017, magnetometer calibration has been viewed as one of the important tasks during the mission operation. This paper is concerned with the in-flight magnetometer calibration which will naturally be influenced by the variation of temperature during the course of orbiting around the earth. A temperature-dependent magnetometer model is proposed and a particle swarm optimization method is adopted in the estimation of calibration parameters. The proposed model and method are verified and tested by using in-flight data from PHOENIX. It is shown that the use of the proposed model together with the optimization method renders a closer match between the magnitudes of the measurement vector and IGRF model. Additionally, the calibration method can be extended to find the suboptimal solution for the satellites with magnetometers without temperature compensation. The proposed approach is believed to be beneficial for small satellites and CubeSats that rely on magnetometer data for attitude determination, orbit determination, and attitude control.

1. INTRODUCTION

Nowadays, 3-axis magnetometers are widely used in the technologies of navigation, inertial sensing and other fields as it can be miniaturized and integrated with other sensors. In the development of CubeSats, owing to the features of small size and low costs, magnetometers have been generally utilized as a sensor for attitude determination and control subsystem (ADCS). Furthermore, the sensor can provide both orientation and magnitude of ambient magnetic field in body frame, these measurements then can be compared with the International Geomagnetic Reference Field (IGRF) model in the reference frame for estimating the attitude, angular rate and orbit of satellite in real time. Most importantly, magnetic sensors can constantly give measurements during the whole orbit period, unlike sun and nadir sensors which only work in sunlit parts of the orbit.

For PHOENIX CubeSat, magnetometer plays a significant role not only in attitude determination but also in attitude control. For example, B-dot control law needs only the rate of change of magnetic field measurements. Therefore, it's important that the performance of ADCS of PHOENIX is strongly related to the accuracy of 3-axis magnetometers. With the pursuit of more accurate measurements, it motivate several studies of magnetometer calibration during the pre-launch and in-flight scenario. This paper mainly describes a method for in-flight magnetometer calibration, which considers no attitude information is available. The objective of attitude-independent magnetometer calibration is to minimize the difference between the magnitudes of the calibrated measurements and the IGRF model. This is done by using several optimization methods. However, the raw measurements of the magnetometer are generally corrupted by the sources, such as fabrication errors, external magnetic field disturbances and temperature-related properties. The accuracy of the measurements basically depends on the knowledge of calibrated parameters. In this study, particle swarm optimization (PSO) algorithm is implemented to estimate 12 parameters, including bias, scale factors, misalignment terms and three temperature-dependent terms.

This paper is organized into section as follows. Subsection 1.1 will present the mathematical model of magnetometers with the explanation of sources of errors and temperature dependent property. Subsection 1.2 briefly describes about the existing calibration algorithms, and the inherent advantage of PSO-based

algorithm will be explained. Then Section 2 will introduce the algorithm of PSO-based magnetometer calibration. Followed by the in-flight verification with actual data from PHOENIX in Section 3. Finally, conclusion will be made in Section 4.

1.1 Mathematical model of magnetometers

Sources of measurement errors can be categorized into the external and internal errors[1]. About external errors, in the actual situation, the in-situ measurements will be influenced by additional magnetic field, which comes from surrounding components. These magnetic perturbations are known as hard and soft iron errors, which make unwanted bias, scale factors and nonorthogonality errors to the raw measurements. In addition, some studies have considered about the effect of time-varying electromagnetic field generated by sources like solar panel currents in sunlit parts of the orbits and magnetic hysteresis of the magnetoquers[2][3]. Thus, additional coefficients and coupling matrix need to be specified to map the magnitude of specific currents and dipole moment vector into time-varying bias (see Ref. [2], [3] for more detail introduction).

On the other hand, internal errors are the errors produced by the instrument itself, which relate to the fabrication errors, characteristics of magnetic materials and even the principle of measurement. For example, Anisotropic Magnetoresistive (AMR) Sensors measure the strength of magnetic field, which rely on the voltage difference of the Wheatstone bridge with four AMR components. The voltage offset results in measurement bias, and scale factor errors relate to the transformation between strength of magnetic field and output voltage. Nonorthogonality errors are caused by misalignment of 3-axis AMR fabrication. In addition, the temperature dependent property of AMR sensors is highlighted in this paper. Due to the small dimensions, the magnetic sensing elements are highly susceptible to temperature effect. Based on the characteristics of resistors, the resistance values will vary as the change of the temperature, which in turn will output erroneous voltage difference in the Wheatstone bridge in the same magnetic environment. Thus, the temperature-dependent terms in the calibration model will be developed in accordance to formula similar to the temperature-dependent resistors.

The overall mathematical model of magnetometers can be derived as below:

$$B_{raw} = (\boldsymbol{S} + \boldsymbol{M})^{-1}((I + S_{si})B_{true} + b_{hi} + \boldsymbol{b} + \varepsilon) \tag{1}$$

where $\boldsymbol{S}$ is a 3×3 diagonal matrix of scale factors, $\boldsymbol{M}$ is a 3×3 zero-diagonal symmetric misalignment matrix, $\boldsymbol{b}$ is a 3×1 vector of bias, I is 3×3 identity matrix, S_{si} represent a 3×3 matrix of soft iron errors and b_{hi} is a 3×1 vector of hard iron bias. All the elements map the error-free magnetic field B_{true} to the raw magnetic measurement B_{raw} with ε as zero-mean Gaussian noise in 3-axis. In this paper, soft and hard iron errors are modeled as measurement noise, and time-varying errors are not considered. To model the temperature-dependent property, three variables α, β and γ are introduced as the temperature coefficients of scale factors, misalignment terms and bias. Therefore, after expansion and simple manipulation, the calibration model of magnetometer becomes

$$\begin{aligned} B_{true} &= B_{calib} - \boldsymbol{\eta} \\ B_{calib} &= \mathbf{A}B_{raw} - \mathbf{d} \end{aligned} \tag{2}$$

, with

$$\begin{aligned} \mathbf{A} &= \boldsymbol{S}_0 + \alpha(T - T_0) + \boldsymbol{M}_0 + \beta(T - T_0) \\ \mathbf{d} &= \boldsymbol{b}_0 + \gamma(T - T_0) \\ \boldsymbol{\eta} &= S_{si}B_{true} + b_{hi} + \varepsilon \end{aligned} \tag{3}$$

where $\boldsymbol{S}_0$, $\boldsymbol{M}_0$ and $\boldsymbol{b}_0$ represent the scale factors, misalignment terms and bias under constant temperature reference T_0. Notice that the calibration model requires the information of in-situ temperature measurements T. Finally, all the 12 calibrated parameters need to be estimated to minimize the difference between magnitude of B_{calib} and B_{true} with combined measurement noise $\boldsymbol{\eta}$.

1.2 Review of attitude-independent calibration

Firstly, with no knowledge of attitude matrix, calibration can only work with scalar measurements. Therefore, the adjusted model becomes:

$$\begin{aligned} \left| C_{orbit}^{body} B_{orbit} \right|^2 &= \left| B_{calib} \right|^2 + \nu \\ \nu &= -2B_{calib}^{T}\boldsymbol{\eta} + |\boldsymbol{\eta}|^2 \end{aligned} \tag{4}$$

where C_{orbit}^{body} represents the rotational matrix that transform B_{orbit} geomagnetic-reference vectors from the orbit frame to the sensor-body frame. Based on similar scalar observation models, numerous algorithms for attitude-independent magnetometer calibration have been proposed with various optimization methods and extensions.

With an objective to minimize the sum of squares of norm residuals, two-step least-square method with batch of measurements has been applied to estimate the intermediate variables, then the calibrated parameters

are extracted by solving algebraic equations[4][5]. Based on the implementation of pseudo-inverse, the optimal intermediate variables can be simply estimated, instead, suboptimal calibrated parameters are not easily transferable with full nonlinear models. Moreover, it had been indicated that if the geomagnetic field is time-varying, recursive process can refine the performance of minimization.

In other study, based on maximum likelihood method, well-known TWOSTEP has been comprehensively extended to estimate bias, scale factors and nonorthogonality terms[6]. To deal with quartic cost function, centering method is utilized to find the initial estimation of intermediate variables with a derived quadratic function, then full cost function is considered to compute the corrected parameters iteratively by Gauss-Newton minimization with the initial estimation. With the assumption of Gaussian and white measurement noise for centering approximation method, TWOSTEP provides a statistically consistent and robust estimation of calibrated parameters even with mis-modeled noise. Further related extension has been made for the purpose of real-time calibration based on similar models and the implementation of extended Kalman filter (EKF) and unscented Kalman Filter (UKF)[7].

In addition to the gradient-method-based calibration, the implementation of PSO-based magnetometer calibration has been widely proposed[8][9]. It has demonstrated the features of fast realization and being insensitive to initial estimate. Owing to the property of stochastic initialization and behavior of swarm intelligence, PSO-based calibration shows the flexibility and convergence-guaranteed capability for various nonlinear model with multi-objective cost function. Moreover, calibrated parameters can be solved directly without conversion from intermediate variable. In this paper, PSO-based algorithm is utilized and extended to solve the temperature-dependent calibration model with 12 parameters. The detail of the PSO-based calibration will be presented below.

2. PARTICLE SWARM OPTIMIZATION

The basic concept of PSO algorithm is to find a particle that perform the best fitness value among the swarm of particles. In addition, each particle will intend to search for a "position" with better solution after moving through a distance, namely, integral of "velocity". More specifically, position of each particle represents a potential solution, while velocity reflect the tendency of moving to a better position in the solution space. To sum up, the process of a typical PSO-based magnetometer calibration consists of three main parts, particles initialization, evaluation and update, which are described in following subsections.

2.1 Particles initialization

The structure of particle swarm needs to be defined in the beginning, including the size of particle swarm n_p and dimension of solution space n_s (length of calibrated parameters). In this paper, the position and velocity of each particle are denoted by $\mathbf{P}_i$ and $\mathbf{V}_i$ as follows.

$$\begin{aligned} \boldsymbol{P}_i(k) &= [P_{i1}(k), P_{i2}(k), ..., P_{in_s}(k)] \\ \boldsymbol{V}_i(k) &= [V_{i1}(k), V_{i2}(k), ..., V_{in_s}(k)] \end{aligned} \tag{5}$$

where subscript "*i*" represents the index of each particles within the range of n_p, while *k* represents the number of iteration. The boundary of solution space can also be defined to adequately constrain the searching range, then initial position and initial velocity of each particle can be generated randomly as below.

$$\begin{aligned} \boldsymbol{P}_i(0) &= P_{\min} + \text{rand}(0,1)\cdot(P_{\max} - P_{\min}) \\ \boldsymbol{V}_i(0) &= -V_{\max} + \text{rand}(0,2)\cdot V_{\max} \end{aligned} \tag{6}$$

,where

$$V_{\max} = \frac{P_{\max} - P_{\min}}{\boldsymbol{V}_{\lim}} \tag{7}$$

Particles are uniformly distributed on positions within the preliminary setting of the boundary. Here, $\boldsymbol{V}_{\lim}$ gives the flexibility to adjust the precision of searching distance during each iteration. Note that the two directions of velocity allow better fitness values to be explored outside the range of initial boundary.

2.2 Particles evaluation

At this stage, the fitness values for each particle will be calculated according to the evaluation of objective function as below:

$$\begin{aligned} Fitness(P_i(k)) &= \sqrt{\frac{1}{m}\sum_{j=1}^{m} Error_j(P_i(k))^2} \\ Error_j(P_i(k)) &= \left|B_{igrf}\right|_j - \left|B_{calib}(P_i(k))\right|_j \end{aligned} \tag{8}$$

where subscript "*j*" represents the index of each measurement and index of corresponding geomagnetic-reference vector from IGRF model, which is within the range of *m* (total number of measurements). PSO-based calibration provides the flexibility for the various representations of error or interested fitness functions. In this paper, root mean square (RMS) error is considered as the evaluation criteria to be minimized. Later, the position of particle with the best fitness value among all particles is selected and denoted as G_{best} and also record the best position for each particle during its

own iteration history denoted as $P_{i,best}$, mathematically written as

$$P_{i,best}(k) = \arg \min_{k=[1,2,\ldots,k]} (Fitness_i(P_i(k)))$$
$$G_{best}(k) = \arg \min_{i=[1,2,\ldots,n_p]} (Fitness_i(P_{i,best}(k))) \quad (9)$$

On each iteration, numerous $P_{i,best}$ are evaluated first, then G_{best} is selected as a position with the minimum fitness value among the determined $P_{i,best}$.

2.3 Particles update

Before updating the positions of each particle, judgement for stopping the iteration has to be determined based on the pre-defined constraints, such as achieving the acceptable fitness value or exceeding the maximum number of iteration k_{max}. If the conditions are not met, positions of particles will be updated with the formula written as

$$\begin{aligned} \boldsymbol{P}_i(k+1) &= \boldsymbol{P}_i(k) + \boldsymbol{V}_i(k+1) \\ \boldsymbol{V}_i(k+1) &= w \cdot \boldsymbol{V}_i(k) \\ &\quad + c_1 \cdot \text{rand}(0,1) \cdot (P_{i,best} - \boldsymbol{P}_i(k)) \\ &\quad + c_2 \cdot \text{rand}(0,1) \cdot (G_{best} - \boldsymbol{P}_i(k)) \end{aligned} \quad (10)$$

by introducing three related coefficients, inertia weight w, cognitive learning rate c_1 and social learning rate c_2. Pre-defined magnitude of inertia weight will determine that particles can escape from the local optimal for the global search or reinforce the precision for the local search. Meanwhile, adequate setting of cognitive and social learning rate facilitate faster converging rate, and also the tendency toward weighted center of $P_{i,best}$ and G_{best}.

Fig. 1 shows the overall procedure of PSO-based magnetometer calibration algorithm. After stopping the iteration, PSO will return the optimal solution G_{best}, which is a combination of calibrated parameters. Further extensions of PSO-based algorithm can be found in Ref. [9], like refinement process and dynamic weighting. This paper will primarily focus on the improvement with temperature compensation, and PSO-based algorithm shows its convergence-guaranteed capability and flexibility with extended magnetometer calibration model.

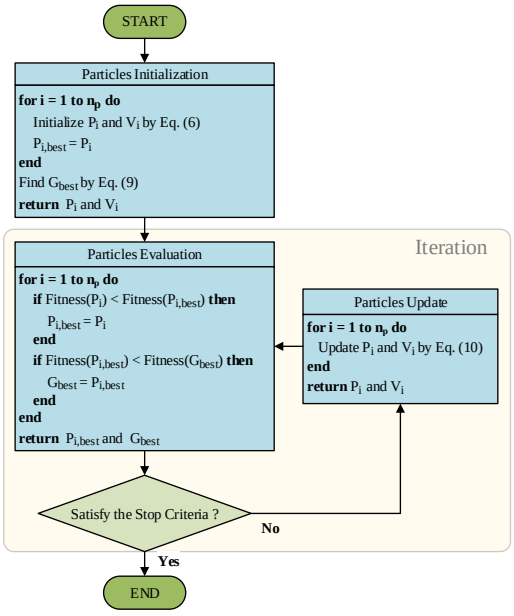

Figure 1: Flowchart of PSO Algorithm

3. INFLIGHT VERIFICATION

To verify the proposed in-flight magnetometer calibration with temperature compensation, PHOENIX CubeSat is viewed as an experimental platform in low earth orbit (LEO), under altitude of 400 km., with inclination about 51.6 degrees. The following subsections will explain the scenario of in-flight verification, the implementation of post-calibration and observation from in-flight experiment with calibrated parameters, then make comprehensive discussions.

3.1 Preliminary statement

PHOENIX CubeSat is equipped with a 3-axis magnetometer, HMC-1053, which is a 3-axis AMR magnetic sensor. However, there is no available temperature measurement within the vicinity of the magnetometer, obtainable readings and locations of other temperature sensors are shown in Fig. 2 and Fig. 3 as below.

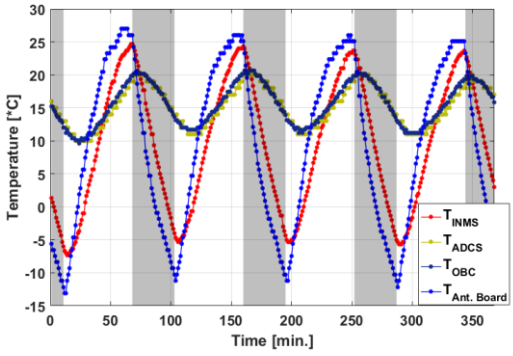

Figure 2: In-Flight Temperature Measurements

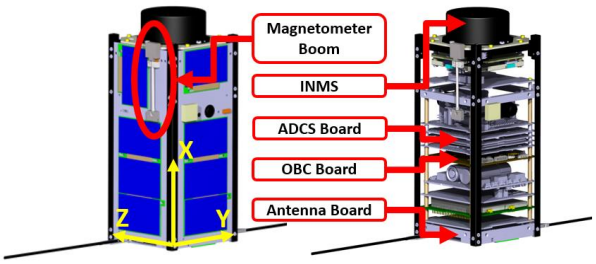

Figure 3: Locations of Thermometers

The shadow areas in Fig. 2 represent that the satellite was in the eclipse parts of the orbit. Obviously, internal measurements (OBC and ADCS boards) perform delayed increase of temperature when getting into sunlit parts of the orbits due to the indirect effect of solar radiation. In contrast, measurements, which are close to the outer panels (Antenna boards and INMS module), are more sensitive to the influence of space environment when orbiting around the earth. In addition, it should be noted that magnetometer is attached to one of the side panels in –Y direction within an aluminum enclosure. Therefore, for PHOENIX, to study the temperature dependency of magnetometer measurements, indirect temperature information will be experimentally applied to the magnetometer calibration, which still leaves uncertainties in calibrated parameters, and temperature coefficients especially.

Consequently, several batches of data, roughly about 370 raw measurements of the 3-axis magnetometer and thermometers with 1 minute intervals fore each, are considered for calibration. Moreover, data will be collected under the scenario of no attitude control applied with mild tumbling (2~3 deg./sec.), which uncertainties of coupling effect from magnetic actuators can be ignored and the temperature can be distributed averagely on each surface of satellite. Fig. 4 shows the magnitude of raw magnetometer measurements and IGRF reference vector from one batch of data.

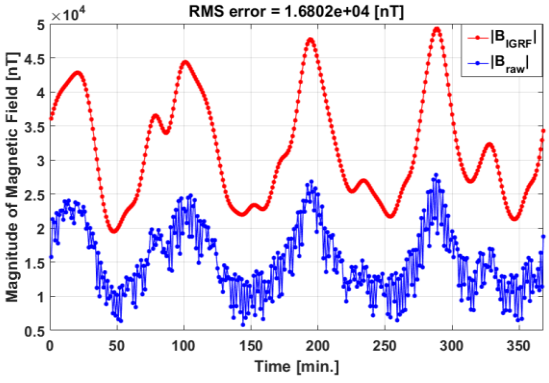

Figure 4: Magnitude of Raw Magnetometer Measurements and IGRF model

3.2 Post-Calibration

As mentioned in Section 2, the objective of PSO-based magnetometer calibration is to find the best calibrated parameters to minimize the RMS error between the magnitude of geomagnetic reference vector and the calibrated magnetic field. According to Eq. (3), the positions of each particle can be set and written as

$$\boldsymbol{P}_i(k) = [S_{11,i}, S_{22,i}, S_{33,i}, M_{12,i}, M_{13,i}, M_{23,i}, b_{1,i}, b_{2,i}, b_{3,i}, \alpha_i, \beta_i, \gamma_i] \tag{11}$$

, which correspond to calibration matrix and vector

$$\mathbf{A}_i = \begin{bmatrix} S_{11,i} & M_{12,i} & M_{13,i} \\ M_{12,i} & S_{22,i} & M_{23,i} \\ M_{13,i} & M_{23,i} & S_{33,i} \end{bmatrix} + (T - T_0) \begin{bmatrix} \alpha_i & \beta_i & \beta_i \\ \beta_i & \alpha_i & \beta_i \\ \beta_i & \beta_i & \alpha_i \end{bmatrix} \tag{12}$$

$$\mathbf{d}_i = \begin{bmatrix} b_{1,i} \\ b_{2,i} \\ b_{3,i} \end{bmatrix} + (T - T_0) \begin{bmatrix} \gamma_i \\ \gamma_i \\ \gamma_i \end{bmatrix}$$

where the scalar term, $T–T_0$, is assumed to be equal along 3-axis direction. It should be noted that the constant T_0 is adjustable, and the adequate setting will be discussed in the later section. Following which post-calibrated magnetic field can be obtained from Eq. (2). A total of 12 calibrated parameters subject to the fitness function from Eq. (8) needs to be optimized. In addition, with the knowledge of pre-flight calibration and specification of the magnetometer, the boundary of solution space can be estimated initially. The preliminary setting of $P_{\max}$ and $P_{\min}$ are specified as below.

$$\begin{aligned} P_{\max} &= [2.3,\ 2.3,\ 2.3,\ 0.3,\ 0.3,\ 0.3, \\ &\quad 7000,\ 7000,\ 7000,\ 10,\ 1,\ 1] \\ P_{\min} &= [2.0,\ 2.0,\ 2.0,\ -0.3,\ -0.3,\ -0.3, \\ &\quad 0,\ 0,\ 0,\ -10,\ -1,\ -1] \end{aligned} \tag{13}$$

Particle swarm can be initialized by Eq. (6) and (7). Other relevant parameters for PSO applied in this paper are listed in Table 1.

Table 1. Parameters for PSO-Based Calibration

Parameter	Value	Description
n_p	100	Size of particle swarm
n_s	12	Dimension of solution space
$\boldsymbol{V}_{\lim}$	100	Constant for velocity limitation
w	0.5	Inertia weight
c_1	1.5	Cognitive learning rate
c_2	1.5	Social learning rate
T_0	0	Reference Temperature [°C]
$k_{\max}$	200	Maximum number of iteration constraint

Moreover, to compensate the temperature-dependent error, measurements from four different thermometers are considered to the magnetometer calibration experimentally. Fig. 5 shows the magnitude errors between IGRF reference vectors and results of post-calibration with four different sources of thermometers, and those errors are analyzed in Table 2. Obviously, one can observe the periodical change of errors, which is caused by the difference between the exact temperature of magnetometer and temperatures in other parts of satellite. Similar situation arise for the calibration without temperature-dependent model considered (a comparison test and denoted as $\mathbf{T_{NONE}}$ in this paper), and its error change periodically as the variation of temperature shown in Fig. 2. In addition, among four thermometers, calibration with temperature in the antenna board performs the minimum RMS error in Table 2, which means the characteristic of temperature measurements are more similar to how exact temperature changes in the magnetometer. Therefore, in the following in-flight verification, temperature measurements in the antenna board will be mainly applied to the magnetometer calibration.

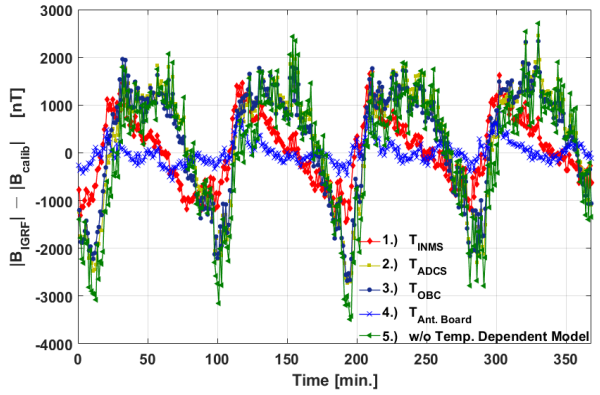

Figure 5: Magnitude Errors of Calibration with Different Temperature Measurements and Calibration without Temperature-Dependents Model Considered (Comparison Test)

Table 2. Analysis of the Errors in Figure 5.

	Source	RMS [nT]	Mean [nT]	STD [nT]
1.	T_{INMS}	710	55.54	709
2.	T_{ADCS}	1240	282.35	1209
3.	T_{OBC}	1194	249.32	1170
4.	$T_{Ant.\ Board}$	234	-0.48	234
5.	$\mathbf{T_{NONE}}$	1296	62.17	1296

Finally, the calibrated parameters are listed in Table 3, which are the results from 50 runs of PSO-based calibration with temperature in the antenna board.

Table 3. Estimation of Calibrated Parameters

Parameter	Estimated	3σ
$[S_{11}, S_{22}, S_{33}]$	[2.064, 2.084, 2.073]	[0.005, 0.002, 0.006]
$[M_{12}\ M_{13}, M_{23}]$	[0.038, 0.1210, -0.015]	[0.002, 0.003, 0.003]
$[b_1, b_2, b_3]$	[5848, 4495, 4841]	[60, 118, 160]
α	0.0066	0.0002
β	0.000202	0.0002
γ	1.246	3.945

3.3 In-flight experiment

In this section, performance of the magnetometer post-calibration will be tested with new runs of in-flight data. To directly evaluate the post-calibrated parameters, it will be uploaded to PHOENIX after each ground-calibration, including bias, scale factors and misalignment terms (PHOENIX has no mechanism of temperature compensation). Therefore, in-flight calibrated measurements can be collected, and complete verification can be done by re-calibrating with in-flight temperature measurement. Fig 6 shows the magnitude error of calibrated in-flight measurement without temperature compensation (as Case 1.), results of re-calibration with temperature measurements (as Case 2.) and results of re-calibration with parameters from the comparison test (as Case 3.). The mean and standard deviation of errors are listed in Table 4.

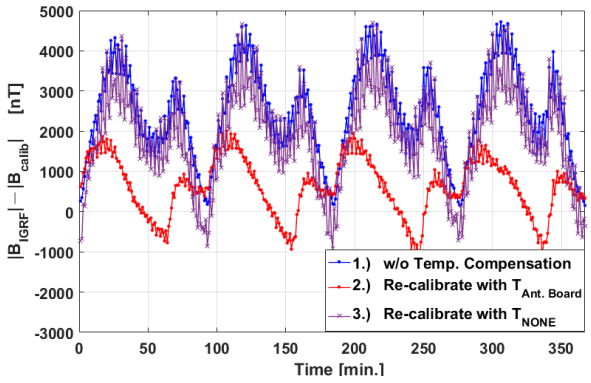

Figure 6: Test with New Runs of In-Flight Data: Magnitude Errors of Calibration with 1.) Only Bias, Scale Factors and Misalignment terms. 2.) All Calibrated Parameters and $T_{Ant.\ Board}$. 3.) Parameters from Comparison Test (T_{NONE}).

Table 4. Analysis of the Errors in Figure 6.

	Description	RMS [nT]	Mean [nT]	STD [nT]
1.	w/o Temp.	2713	2456	1153
2.	w/ $T_{Ant.\ Board}$	941	607	720
3.	w/ $\mathbf{T_{NONE}}$	2226	1868	1214

For the calibration without temperature compensation (Case 1.), fixed bias, scaler factors and misalignment terms primarily make the magnitude errors greatly change with not only temperature in the device but also the magnitude of true magnetic field, and result in the periodical errors with a specific pattern. On the other hand, with the uncertainty of the exact temperature in the magnetometer, the result of re-calibration with temperature in antenna board shows larger RMS error than the result of post-calibration in the previous subsection. It's not only the issue of non-global optima for the magnetometer calibration, but also the concern about the indirect temperature input for temperature-dependent model during the calibration. The relation between the exact temperature in the magnetometer and in other parts of satellite is highly complicated and even attitude-related. It means the calibrated parameters will suffer from the uncertainty of hardly observable transformation from indirect temperature ($T_{Ant.\ Board}$) to exact temperature ($T_{magnetometer}$) measurements, and result in the optima for the calibration with specific batch of data. Therefore, the calibration with different batch of data input may shows not only variable temperature coefficients but also inconsistent terms of bias, scale factors and misalignment. However, take the comparison between fixed bias, scale factors and misalignment terms from the calibration with indirect temperature (Case 1.) and the calibration without temperature-dependent model (Case 3.), the latter ones show larger scale of variation in Fig. 6. The jittering points in Fig. 6 are caused by errors in calibrated parameters with different attitude of satellite. Because parameters in Case 1 are optimized with the consideration of filtering the temperature dependent characteristics, it perform more robustly than Case 2 under the same effect of temperature.

Eventually, the in-flight experiment basically shows the improvement with temperature compensation despite the indirect temperature measurements experimentally applied. The uncertainty in calibration with indirect temperature compensation can be addressed if exact temperature measurements in the magnetometer are available.

3.4 Extended study

The study can be extended to find suboptimal solution for magnetometers without mechanism of temperature compensation based on the decision of temperature reference T_0 in Eq. (3). For the in-flight calibration without temperature compensation, magnitude of calibrated results will be influenced by the temperature dependent terms during orbiting around the earth. However, the magnitude of those terms can be reduced if the temperature inputs are close to the pre-defined T_0 in the calibration model. Fig. 7 shows the magnitude errors of calibration with different setting of T_0, and the magnitudes of temperature dependent terms are included to simulate the condition of no temperature compensation.

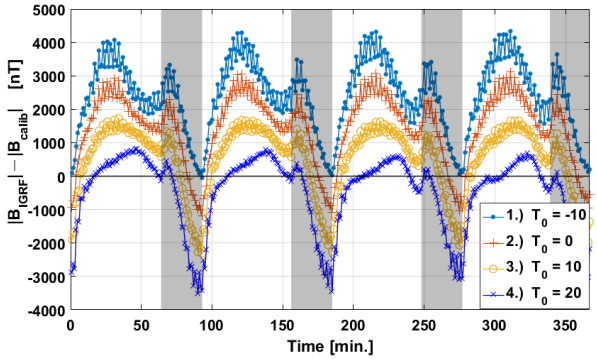

Figure 7: Magnitude Errors of Calibration with Different Setting of T_0 and Including the Magnitude of Temperature Dependent Terms.

Table 5. Analysis of the Errors in Figure 7.

	T_0 [°C]	RMS [nT]	Magnitude of Errors < 1000 [nT]
1.	–10	2630	14.4 %
2.	0	1780	23.9 %
3.	10	1156	43.0 %
4.	20	1188	76.2 %

Obviously, different setting of T_0 will have the corresponding value of $\boldsymbol{S}_0$, $\boldsymbol{M}_0$ and $\boldsymbol{b}_0$ in Eq. (3), and results in different performance of error as the temperature changes. In this paper, among the four settings of T_0 in the Fig. 7, blue line, T_0 = 20 °C, is viewed as the best solution, because it has the larger proportion of the acceptable errors (despite it's not the minimum RMS errors). The results and the setting of T_0 can be expected and observed initially with the information of temperature variation. If most of temperature measurements are distributed nearby the pre-defined T_0, it generally perform smaller magnitude of temperature dependent terms. Moreover, it also gives the possible reason for the requirement of magnetometer calibration as a regular work for PHOENIX (especially for magnetometers without temperature compensation), because the distribution of temperature in space will vary with the different beta angle, which effects the proportions of sunlit and eclipse duration in each orbit.

Consequently, further suboptimal solution can be completed by expending the dimension of solution space for PSO-based calibration and optimizing the temperature reference T_0. Specific fitness function or multi-objective functions can be defined to satisfy different pursuit of performance.

4. CONCLUSION

The study gives an insight into magnetometer calibration with its temperature-dependent property. A temperature-dependent magnetometer model is derived with the similar formula of temperature-dependent resistors. To complete the full calibration, raw magnetic field measurements, actual temperature in the magnetometer and expected magnitude of IGRF model are required. The calibrated parameters are estimated using the PSO-based calibration with the goal of minimum RMS of errors. The optimization algorithm shows its features of flexibility for different definition of fitness function, convergence-guaranteed capability with pre-defined boundary of solution space and the advantage that calibrated parameters can be computed directly.

Because of the lack of exact temperature information in the magnetometer, indirect temperature measurements are experimentally applied to the proposed calibration method. The results of calibration perform the significant improvement in comparison with no temperature-dependent model is considered in the calibration. Nevertheless, the calibration with the use of indirect temperature input still remains uncertainty in the estimation of calibrated parameters, which affects the performance of in-flight verification. Magnitude errors from the in-flight test are inconsistent with the expected results from the PSO-based calibration. However, it should be noted that the terms of bias, scale factors and misalignment from proposed calibration method still show more robust performance in comparison with calibration without temperature-dependent model. Further complete analysis of in-flight verification can be achieved if exact temperature measurements in the magnetometer are available. Moreover, another contribution of this paper is to represent the method for finding suboptimal solution for satellites with magnetometer without temperature compensation, based on the appropriate setting of T_0 in the calibration model.

For small satellites and CubeSats that rely on the application of magnetometers, and even magnetometers without temperature compensation, the proposed approach is believed to give improved and robust performance of in-flight calibration under the scenario of various temperature during orbiting the earth.

5. ACKNOWLEDGEMENTS

The author would like to thank Prof. Jyh-Ching Juang for his instruction and support during experiment operation for PHOENIX. Also, the author acknowledge all students who contributed to the development of PHOENIX CubeSat. Especially, the great support from von Karman Institute (VKI), who manages the QB50 project, and all participants are very appreciated.

6. REFERENCES

1. Valérie Renaudin, Muhammad Haris Afzal and Gérard Lachapelle, “Complete Triaxis Magnetometer Calibration in the Magnetic Domain”, Journal of Sensors, vol. 2010, article ID 967245.
2. John C. Springmann and James W. Cutler, “Attitude-Independent Magnetometer Calibration with Time-Varying Bias”, Journal of Guidance, Control and Dynamics vol. 35, No. 4, July-August 2012.
3. Eugnhyun Kim, Hychoong Bang and Seon-Ho Lee, “Attitude-Independent Magnetometer Calibration Considering Magnetic Torquer Coupling Effect”, Journal of Spacecraft and Rockets, vol. 48, No. 4, July-August 2011.
4. LIU Zhiping and XUE Jinqiang, “New Calibration and Error Compensation for Strapdown Magnetometer”, Proceedings of the 34th Chinese Control Conference, July 28-30, 2015.
5. Christopher C. Foster and Gabriel Hugh Elkaim, “Extension of a Two-Step Calibration Methodology to Include Nonorthogonal Sensor Axes”, IEEE, Transactions on Aerospace and Electronic Systems, vol. 44, No. 3, July 2008.
6. Roberto Alonso and Malcolm D. Shuster, “Complete Linear Attitude-Independent Magnetometer Calibration”, Journal of the Astronautical Sciences, vol. 50, No. 4, October-December 2002.
7. John L. Crassidis and Kok-Lam Lai, “Real-Time Attitude-Independent Three-Axis Magnetometer Calibration”, Journal of Guidance, Control and Dynamics, vol. 28, No. 1, January-February 2005.
8. Z. Wu, Y. Wu, X. Hu and M. Wu, “Calibration of Three-axis Strapdown Magnetometers Using Particle Swarm Optimization Algorithm”, Proceedings of IEEE International Symposium on Robot. Sensors Environment, 2011.
9. Bagus Adiwiluhung Riwanto, Tuomas Tikka, Antti Kestilä and Jaan Praks, “Particle Swarm Optimization with Rotation Axis Fitting for Magnetometer Calibration”, IEEE Transactions of Aerospace and Electronic Systems, vol. 53, No. 2 April 2017.